

Arcturus: A Cloud Overlay Network for Global Accelerator with Enhanced Performance and Stability

Matthew Yang Liu¹, Chuang Chen², Pengcheng Lv², Hui Guo², Yanan Zhang², Cong Wang²,
Yusen Li³, Zhenyu Li⁴, Yu-Chu Tian⁵

¹Bilibili Inc., ²Tianjin University of Science and Technology, ³Nankai University,
⁴ICT, CAS, ⁵Queensland University of Technology

Abstract

Global Accelerator (GA) services play a vital role in ensuring low-latency, high-reliability communication for real-time interactive applications. However, existing GA offerings are tightly bound to specific cloud providers, resulting in high costs, rigid deployment, and limited flexibility, especially for large-scale or budget-sensitive deployments. *Arcturus* is a cloud-native GA framework that revisits the design of GA systems by leveraging low-cost, heterogeneous cloud resources across multiple providers. Rather than relying on fixed, high-end infrastructure, *Arcturus* dynamically constructs its acceleration network and balances performance, stability, and resource efficiency. To achieve this, *Arcturus* introduces a two-plane design: a forwarding plane that builds a proxy network with adaptive control, and a scheduling plane that coordinates load and routing through lightweight, quantitative optimization. Evaluations under millions of RPS show that *Arcturus* outperforms commercial GA services by up to 1.7× in acceleration performance, reduces cost by 71%, and maintains over 80% resource efficiency—demonstrating efficient use of cloud resources at scale.

1 Introduction

Unlike traditional Content Delivery Networks (CDNs) [58] and live streaming [47], Global Accelerator (GA) constructs a dynamic proxy network to optimize end-to-end data transmission, with widespread adoption in real-time interactive applications, including cloud gaming [77], online education [1], and mobile office applications [54], etc. As a premium value-added service built upon Elastic Compute Service (ECS) or CDN infrastructure, GA commands steep charges. Taking AWS GA as an example, in addition to the base EC traffic costs, users incur additional fees, including an accelerator operation charge of \$0.025 per hour and a DT-Premium fee—for instance, up to \$0.035 per GB for data transfer between the US and the Asia-Pacific region [15].

Currently, GAs are exclusively provided by major cloud providers [13, 33, 78], offering users a seamless interactive

experience. However, in practical deployment, GAs face several challenges. Firstly, GA infrastructure is built upon ECS [13, 33] or CDN [24, 25] networks. The reliance on high-end network hardware results in elevated costs and a rigid billing model. For instance, even in non-critical scenarios like testing, users are required to pay significant fees. Secondly, GA shares its infrastructure with other services (e.g., CDN) [41], making it challenging to implement upgrades or modifications that cater to differentiated demands. For example, a client may require user IP information to be transmitted to the server for statistical purposes, but the shared infrastructure limits such customization. Thirdly, the requirement often mandates the service deployment on resources provided by the accelerator provider, further limiting the scope of acceleration service usage. Fourthly, the edge resource coverage of a single cloud provider is constrained. A single cloud provider typically lacks the resource breadth necessary to ensure wide geographic coverage, particularly in regions such as Southeast Asia and Africa.

The growing availability of low-cost, globally distributed cloud instances—especially from smaller and regional cloud providers—has opened up new opportunities for rethinking GA architectures. These providers offer a wealth of cost-effective resources, making it feasible to construct flexible, scalable GA systems at a fraction of the traditional cost. Nonetheless, this opportunity brings significant challenges due to the heterogeneity of cloud resources and the dynamic nature of GA workloads, which are characterized by high requests per second (RPS) and uneven traffic distribution. These factors complicate the coordination of system responsiveness, operational robustness, and efficient capacity use in a cloud-based GA (§2).

To address these challenges, we present *Arcturus*¹, a self-managed, multi-cloud GA framework that decouples from provider-specific services and leverages heterogeneous cloud infrastructure. *Arcturus* adapts to dynamic runtime conditions while minimizing costs and sustaining high service quality.

¹*Arcturus* is open-sourced on <https://github.com/Bootes2022/Arcturus>, with the entire system comprising over 15K lines of code.

Drawing from the design principles of integrated electrical propulsion systems [35], it maintains a dynamic equilibrium between conflicting performance objectives, ensuring effective and reliable resource use across complex environments.

The *Arcturus* Overview (§3) presents the designs of the forwarding (§3.1) and scheduling (§3.2) planes, emphasizing their key distinctions from traditional data and control planes. These innovations serve as the fundamental framework for *Arcturus* to better accommodate heterogeneous cloud environments and adapt more flexibly to volatile workloads.

In the Forwarding plane (§4), *Arcturus* simultaneously refines data proxying and network routing processes. For data proxying (§4.1), it utilizes streaming multiplexing [7] and packet merging to enhance transmission effectiveness. Additionally, the contextual multi-armed bandit (CMAB) optimizes the parameters of these techniques, thereby maximizing the single-node’s optimal capabilities. Regarding network routing (§4.2), segment routing [6] allows *Arcturus* to execute path-level forwarding with fine-grained control.

For the scheduling plane (§5), *Arcturus* splits into last- and middle-mile stages. The last-mile uses a Lyapunov-based model [56] to balance performance and stability, solved via a fast heuristic (§5.1). The middle-mile prioritizes path diversity by recasting a constrained multi-path problem as a maximum flow problem with conflicts, tackled with the Carousel Greedy algorithm [20] (§5.2).

The Resilience Pillars of *Arcturus* significantly enhance system robustness. The employed mechanisms include path backup, failure recovery, and place-holder backlogs [57] (§6). Collectively, these strategies guarantee high availability and strong fault tolerance. As a result, the network remains stable, even in highly dynamic conditions.

Experimental results show that *Arcturus* consistently maintains over 80% resource utilization while preserving normal service performance under acceleration workloads. When compared to commercial accelerators [13, 33], *Arcturus* enhances acceleration performance by 1.7x and reduces operational costs by 71%, especially when scaling to support millions of RPS (§7).

2 Background & Challenge

Global Accelerator(GA)² GA primarily leverages proximity-based access strategies [22] and segmented routing [59] to provide users with a proxy network that ensures both high acceleration performance and stability.

As shown in Tab. 1, compared to Video-on-Demand (VOD) [80] and live streaming [50], GA’s real-time metadata is smaller in size and requires significantly less bandwidth, in stark contrast to bandwidth-intensive services. However, Figure 1 reveals that the number of proxy requests is both large

²Business-related information on GA is based on technical interactions with our partner cloud vendors.

Table 1: The Average Bw of Requests for Diff Businesses

Bussiness	Global Accelerator	VOD and Live
Average bw(bps)	4K	10,000K

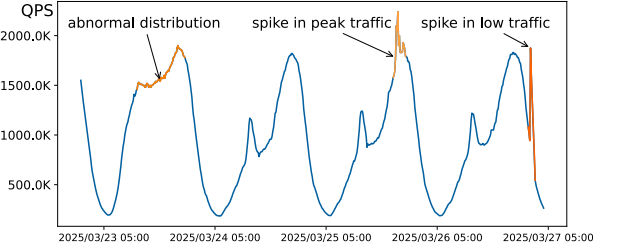


Fig. 1. The RPS Distribution of GA in a certain region over several consecutive days. In the graph, clear distribution anomalies can be observed, along with spikes occurring during both peak and non-peak hours.

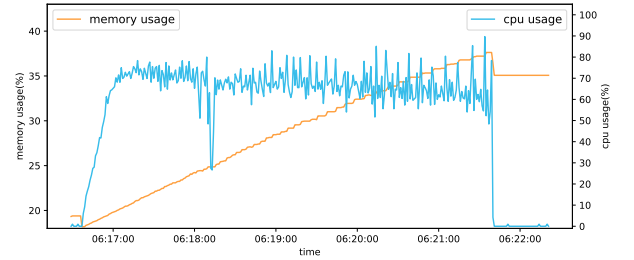


Fig. 2. Resource usage profile (CPU and memory) of small-file acceleration services.

and highly unstable, placing heavy pressure on system operations. As a result, real-world system scheduling strategies must focus on ensuring responsive acceleration and maintaining robust service quality.

From a business perspective, GA functions as a connection-intensive application, which can be viewed as a lightweight form of compute-intensive workloads. As depicted in Fig. 2, a sudden and substantial increase in connection requests can inundate server CPUs with tasks related to connection establishment and data transmission. This inundation causes CPU utilization to spike sharply. Although GA also utilizes memory to maintain connection states, the CPU usually remains the main bottleneck, particularly in small file transfer scenarios, the cost associated with connection handling outweighs the resource consumption caused by the few ms of data processing.

Therefore, this paper excludes the impact of memory, bandwidth, I/O, and other factors on system performance and stability, primarily focusing on CPU-related aspects.

Heterogeneous Cloud Resources. The heterogeneity of cloud resources manifests in multiple dimensions. Previous studies have extensively explored aspects such as pricing [67, 69, 81], reproducibility [70], throughput, and latency [39, 74]. However, most of this research has focused on

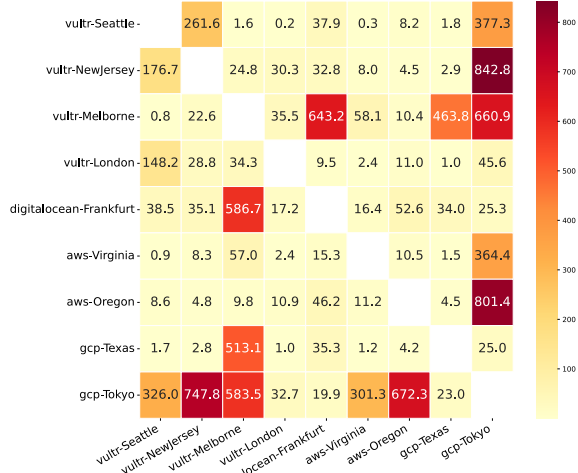


Fig. 3. The Variance of Transmission Delay. We selected multiple geographical locations and constructed a network using two tier-1 cloud providers and two tier-2/3 cloud providers to conduct our measurements.

bandwidth-intensive workloads like video streaming and large-file transfers. In contrast, GA’s average transfer file size is only 512B, and the latency and performance of cloud VM instances (VMs) in small-file transmission scenarios remain underexplored.

Given GA’s proximity-based access mechanism, we prioritize deploying a denser network of low-spec proxy nodes near users over fewer high-performance ones under the same cost constraints. This approach incorporates tier-2/3 cloud providers [27, 72] into our study, diverging from prior research that primarily examined mainstream cloud providers [14, 36, 55]. Thus, our work explores resource combinations across cloud providers of varying tiers.

Fig. 3 presents the variance in network delay recorded over 24 hours for 512B file transfers between nodes from different providers and geographic locations. At approximately 3:15 PM local time, the GCP Tokyo node experienced unidentified outbound network issues, causing widespread timeouts lasting around 15 minutes (Fig. 18). Additionally, the Vultr Melbourne node exhibited frequent and erratic latency fluctuations. After filtering out these two anomalies, our analysis revealed that intra-network Vultr nodes displayed evidently lower stability compared to other providers.

As shown in Fig. 4, we benchmarked the performance of VMs with various configurations from different-tier cloud providers when these VMs were handling small files. While tier-2/3 providers like Vultr and DigitalOcean offer lower prices than tier-1 clouds, they exhibit significantly higher error rates during system bottleneck periods. Moreover, in a surprising comparison, we found that Vultr’s dedicated CPU VMs generally underperformed compared to shared CPU VMs during system bottlenecks.

Challenge 1: HOW CAN CLOUD OVERLAYS SUPPORT

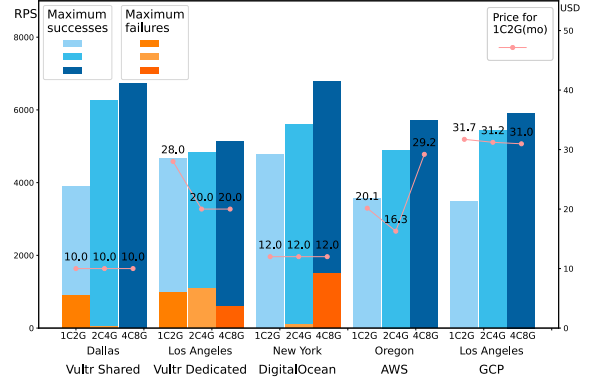


Fig. 4. Benchmarking Cloud Server Performance: Load Testing. The figure depicts the average number of successful RPS and the corresponding failure rates within a short time window around the system’s bottleneck point for diverse server configurations. Additionally, it presents the average monthly cost (USD) per 1C2G resource unit for each configuration.

COMPUTE-INTENSIVE APPLICATIONS? For bandwidth-intensive applications built on overlay networks, the primary concerns are throughput and cost due to their low request frequency and minimal fluctuations. However, designing and implementing compute-intensive applications like GA within an overlay network presents unique challenges, with few established reference solutions.

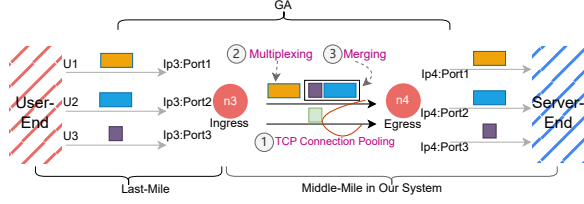
Challenge 2: HOW CAN GA ACHIEVE HIGH PERFORMANCE AND STABILITY AMID CLOUD RESOURCE HETEROGENEITY? Given the performance bottlenecks and heterogeneous nature of cloud resources, along with GA’s compute-intensive characteristics, achieving a high-performance and stable GA within a cloud overlay network while maximizing resource utilization remains a major challenge.

3 Arcturus Overview

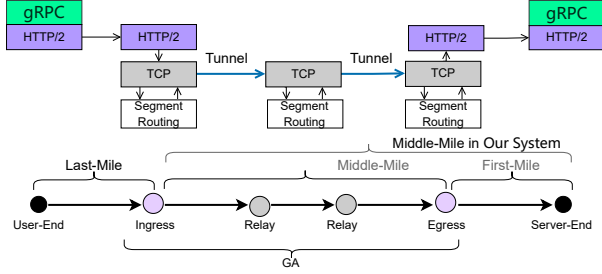
The inherent limitations of SDN’s data and control planes [19], as emphasized in the overview, have motivated the design of more efficient forwarding and scheduling planes, leading to substantial gains in system performance and stability.

3.1 Forwarding Plane

Based on previous experience, there are two main approaches to building proxy nodes. The first is to retrofit existing proxy servers [2, 4, 5], which are often heavily loaded and tightly coupled with complex logic, making it hard to extend them with custom routing and scheduling capabilities. Therefore, we turn to the second solution, which is to develop custom proxies tailored for GA scenarios. Nevertheless, even with custom proxies, we still face numerous obstacles. General-purpose proxy technologies, such as HTTP multiplexing and



(a) **Data Proxying.** The ingress and egress nodes represent user connections by assigning specific ports, while intermediate nodes forward traffic through a unified TCP tunnel.



(b) **Network Routing.** At the ingress and egress nodes, protocol stack unloading and loading are performed, while segment routing is employed within GA to enable packet forwarding.

Fig. 5. Forwarding Architecture.

TCP connection pooling at the protocol layer and eBPF [32] at the kernel layer, offer limited flexibility. For instance, supporting advanced protocols like QUIC [45], which demand high CPU resources, poses a significant challenge for resource-constrained nodes. Moreover, eBPF-based forwarding usually requires host-mode privileges, and it is extremely difficult to obtain these privileges in cloud environments due to the stringent security policies.

Given GA's high RPS and small packet sizes, we implement three key enhancements to build a lightweight, high-performance data proxy tailored to its demanding characteristics, including TCP connection pooling, multiplexing, and small packet merging as shown in Fig. 5a. The first two improve TCP connection utilization, while the third optimizes network resource usage and enhances transmission efficiency.

As shown in Fig. 5b, we use Segment Routing [6] for network routing over the TCP protocol. In contrast, Label-based routing technologies, such as MPLS [60] and LDP [17], introduce complex timing logic for label distribution. Given the fluctuations in cloud networks, improper handling of this timing logic is more likely to cause localized instability, further complicating the maintenance of a reliable system in practical applications. Moreover, segment routing facilitates gradient descent control, enabling fine-grained scheduling and simplifying precise control.

3.2 Scheduling Plane

GA requires not only high-quality path selection but also real-time network awareness, rapid decision-making, and agile

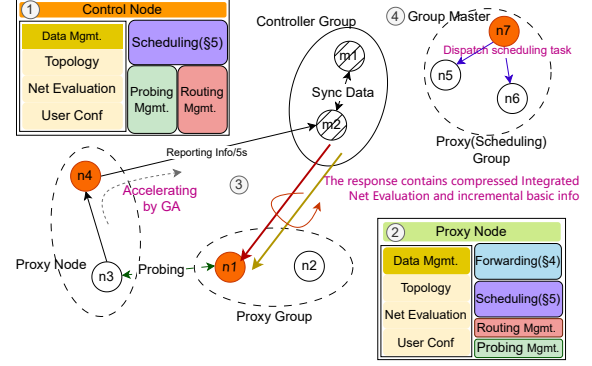


Fig. 6. Scheduling Architecture. The controllers integrate global performance and stability data, compress the results, and synchronize the summary across all nodes. This allows both the controller and proxy nodes to contribute to scheduling decisions.

path switching. Traditional architectures relying on centralized, high-spec control centers have two major drawbacks. First, they lack the responsiveness necessary for timely, fine-grained route adjustment. Second, they are prone to compute bottlenecks, limiting scalability. To address these limitations, we must embrace edge scheduling as the inevitable path forward. However, achieving this requires rapid propagation of the global state across the network. As a result, efficient data synchronization has emerged as a critical challenge for building a scalable and resource-aware scheduling plane.

We handle relatively static data, such as network topology and user configurations, by incrementally propagating them to proxy nodes. However, dynamic metrics like CPU load, memory usage, and latency must be synchronized in real time. Especially, network-wide latency measurement scales quadratically with node count, which hinders scalability in large deployments. Inspired by distributed robust computation [65], we leverage a K-Nearest Neighbors (KNN)-based [38] approach to partition performance data into singular (outlier) and non-singular components. For non-singular components, we only synchronize aggregate statistics like the mean and median. This significantly reduces communication overhead, up to 80% in some cases (Fig. 17). By experimental results, our approach maintains decision accuracy with no noticeable performance degradation.

As shown in Fig. 6, ① and ② illustrate the core data structures and functions of the controller and proxy components. The proxy synchronizes globally compressed data and has the same scheduling capability as the controller. As shown at ③, each proxy node sends its compressed probe data along the GA path to the central controller every 5 seconds—an interval shared by both data sync and computation cycles to mitigate overreaction to network jitter. The controller aggregates and compresses the global state, then distributes the summarized results back to the edge nodes. To reduce compute bottlenecks, nodes are organized into regional schedul-

ing groups—identical to proxy groups by default—using distributed coordination services like *etcd* [3], as illustrated at ④. Each group elects a master node to distribute tasks based on resource availability, improving load balancing and enabling scalable, responsive scheduling across the system.

4 Forwarding

4.1 Enhanced Proxying

Arcturus integrates three key techniques to optimize connection management: TCP connection pooling, stream multiplexing, and packet merging. Rather than detailing each mechanism individually, we focus on their combined effect: reducing connection overhead and enhancing overall throughput while maintaining control over latency. When implementing multiplexing and packet merging, the system must configure key parameters, including the number of multiplexing sessions (S_p), concurrency levels (C_p), and packet merge timeout (T_p). These parameters greatly impact system performance, with their adjustment requiring careful trade-offs between resource consumption and processing capabilities. To address the complex interdependencies and the dynamic nature of network and load conditions in cloud environments, we use the LinUCB [21] algorithm to dynamically optimize these parameters and guide decision-making.

Definition of Bandits and Arms. The number of Bandit arms is determined by three key parameters: S_p , C_p , and T_p . Based on stress testing experience, we define the search ranges for S_p and C_p : $S_p \in [1, 10]$ with a step size of 1, and $C_p \in [50, 200]$ with a step size of 10, which is sufficient to cover more than 95% of the cases observed in practice. For T_p , considering that intercontinental acceleration typically involves two proxy hops and an end-to-end latency of approximately 100 ms, we constrain the additional processing delay introduced by packet merging to within 10% of the total latency. Based on this constraint, the upper bound T_p is set to 5 ms, resulting in a configurable range of 1–5 ms.

Contextual Feature. Experimental results show that the configurations of S_p , C_p , and T_p are strongly correlated with CPU utilization, RPS, the number of requests processed per unit time (RQPT), and average request processing time (ART). Hence, we adopt these four metrics as performance counters, serving as contextual features to guide the exploration of the search space.

Design of Reward. First, we normalize $RQPT$ using its historical minimum and maximum values³: $RQPT_{\text{norm}} = (RQPT - RQPT_{\text{min}}) / (RQPT_{\text{max}} - RQPT_{\text{min}})$. Similarly, we normalize ART as $ART_{\text{norm}} = (ART - ART_{\text{min}}) / (ART_{\text{max}} - ART_{\text{min}})$. The reward is then calculated as $Reward = w_{RQPT} \times RQPT_{\text{norm}} + w_{ART} \times (1 - ART_{\text{norm}})$, which provides a unified optimization signal that balances low-latency processing of individual requests with high overall throughput. Here, w_{RQPT}

³The initial minimum and maximum values are derived from experimental observations.

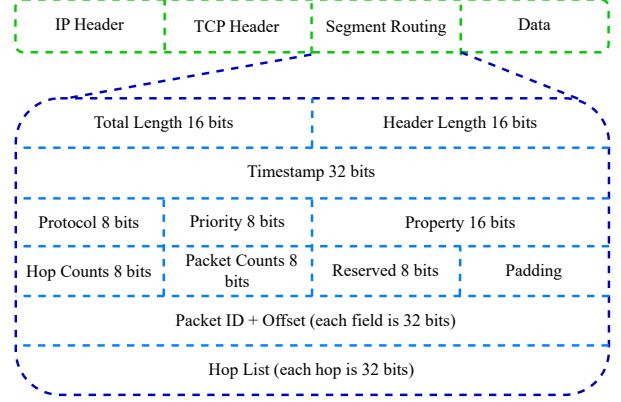


Fig. 7. Segment Routing Header.

and w_{ART} represent the weights for $RQPT_{\text{norm}}$ and ART_{norm} , respectively, with sum 1 and initial values 0.5.

It is important to note that the reward function does not account for stability feedback. This is because when parameter adjustments cause system instability, the Lyapunov drift (Eq.(3)) increases, and the scheduling system will automatically reduce the traffic flow to maintain stability. Thus, the RPS decreases, leading to a natural drop in reward.

4.2 Network Routing

Arcturus adopts segment routing technology based on the TCP protocol for network routing. By designing a custom protocol header that incorporates multidimensional control information, it offers structured support for data control and forwarding. As shown in Fig.7, the protocol header includes essential fields such as packet_id, offset, hop_list, and hop_counts. The packet_id uniquely identifies sub-requests within a merged request, while the offset field specifies the relative position of each sub-request within the merged data, ensuring accurate reconstruction. The hop_list and hop_counts form the routing control mechanism that guides the forwarding behavior of intermediate nodes. This standardized protocol header structure enables proxy nodes to efficiently parse and forward data, significantly reducing the computational overhead on the nodes.

5 Scheduling

The separation of last-mile and middle-mile scheduling strategies reflects their distinct responsibilities. The last-mile directly handles user requests by routing them to proxy groups covering their access regions, demanding higher stability and tighter latency control to ensure availability and user experience [18]. In contrast, the middle-mile forwards aggregated traffic from ingress proxies to service servers across multi-hop paths. While routing is more complex, it benefits from stronger proxy capabilities and is less sensitive to latency. To enhance end-to-end stability, the system exploits path diver-

sity in the middle-mile to dynamically bypass failures and transient congestion.

5.1 Last-Mile Scheduling

5.1.1 Lyapunov Drift and Optimization Modeling

To scheduling regional user requests to proxy nodes, a proxy group consisting of N proxy nodes is considered and modeled as a system of N queues. Let $\mathbf{Q}(t) = (Q_1(t), \dots, Q_N(t))$ denote the queue backlog vector, where $Q_k(t)$ is updated according to Eq.(1) and serves as a virtual stability queue, capturing the cumulative deviation of the average CPU load from a predefined threshold θ , typically set to 60%, the commonly accepted upper limit for balancing utilization and stability, quantifying the long-term stability of the system.

$$Q_k(t+1) = \max \left[Q_k(t) + \underbrace{\text{c}\bar{\text{p}}\text{u}_k^{t,\text{onset}} + \delta\text{c}\bar{\text{p}}\text{u}_k^{t,\text{in}}}_{\text{estimation of c}\bar{\text{p}}\text{u}_k^{t+1,\text{onset}}} - \theta, 0 \right] \quad (1)$$

where $\delta\text{c}\bar{\text{p}}\text{u}_k^{t,\text{in}}$ represents the estimated change in average CPU utilization during slot t , caused by the input rate change $\delta\text{req}_k^{t,\text{in}}$, given the known system state $\text{c}\bar{\text{p}}\text{u}_k^{t,\text{onset}}$. Here, $\text{c}\bar{\text{p}}\text{u}_k^{t,\text{onset}}$ denotes the average CPU utilization in the previous $t-1$ slot, measured at the beginning of slot t .

To enable proactive scheduling, Arcturus estimates CPU utilization changes using a predictive model. Specifically, during time slot t , the estimated change $\delta\text{c}\bar{\text{p}}\text{u}_k^{t,\text{in}}$ is computed by an approximation function $\hat{f}_k(\delta\text{req}_k^{t,\text{in}} | \text{c}\bar{\text{p}}\text{u}_k^{t,\text{onset}})$. In contrast, the actual CPU utilization $\text{c}\bar{\text{p}}\text{u}_k^{t+1,\text{onset}}$, observed at the onset of slot $t+1$, is used to update the queue backlog $Q_k(t+1)$, ensuring accurate state tracking.

The mapping function \hat{f}_k is generally a complex, nonlinear function of multiple system parameters. However, due to the relative stability of cloud hardware performance—especially among identically configured instances— \hat{f}_k can be effectively learned from historical data. The model is initially built as a piecewise empirical approximation and incrementally refined with LSTM-based [71] predictors trained on online data to reflect real-time CPU dynamics. The low input dimensionality improves prediction accuracy as more data accumulates and often exceeds 95% (Fig. 19). Moreover, approximate trends have proven sufficient for scheduling decisions. We leave the pursuit of higher prediction accuracy to future work.

Lyapunov function. As a measure of the "size" of the vector $\mathbf{Q}(t)$, define a quadratic Lyapunov function $L(\mathbf{Q}(t))$ as Eq.(2):

$$L(\mathbf{Q}(t)) = \frac{1}{2} \sum_{k=1}^N w_k Q_k(t)^2 \quad (2)$$

where w_k are a collection of positive weights, typically set as $w_k = 1/C_k$, where C_k is the number of CPU cores on node k ,

e.g., $w_k = 1/4$ for a 4-core node. This weight design reflects heterogeneous node capacity in the system.

Lyapunov drift. Define the one-slot conditional Lyapunov drift $\Delta(\mathbf{Q}(t))$ as Eq.(3):

$$\Delta(\mathbf{Q}(t)) \triangleq \mathbb{E}\{L(\mathbf{Q}(t+1)) - L(\mathbf{Q}(t)) | \mathbf{Q}(t)\} \quad (3)$$

Lyapunov drift refers to the change in the virtual queue between two consecutive time slots, reflecting the trend of system stability. By choosing decisions that minimize the drift, system stability can be ensured.

Theorem 1. Consider the quadratic Lyapunov function Eq.(2), and assume $\mathbb{E}\{L(\mathbf{Q}(0))\} < \infty$. Suppose there is a constant $B > 0$ such that the following drift condition holds for all slots $t \in \{0, 1, 2, \dots\}$ and all possible $\mathbf{Q}(t)$ as Eq.(4) :

$$\Delta(\mathbf{Q}(t)) < B + \sum_{k=1}^N w_k Q_k(t) \cdot \delta\text{c}\bar{\text{p}}\text{u}_k^{t,\text{in}} \quad (4)$$

and all queues are mean rate stable $\lim_{t \rightarrow \infty} \frac{\mathbb{E}\{|Q_k(t)|\}}{t} = 0$.

Proof. See Appendix A. ■

Drift-plus-penalty. Moreover, to optimize the system's performance, it is necessary to not only minimize drift but also consider the penalty of latency. Therefore, latency is introduced, and the weighted sum of drift and latency forms the final drift-plus-penalty (DPP) function as Eq.(5):

$$\Delta(\mathbf{Q}(t)) + V \cdot \mathbb{E}\{\text{delay}(t) | \mathbf{Q}(t)\} \quad (5)$$

The penalty term $\text{delay}(t)$ represents the penalty of latency in slot t , which balances stability and latency through the weight parameter V , optimizing overall system performance.

Lyapunov Optimization. Therefore, we can perform the last-mile scheduling by minimizing the total DPP, and thus we can obtain problem P1 as Eq.(6):

$$\mathbf{P1} : \min_{\delta\text{req}_k^{t,\text{in}}} (\Delta(\mathbf{Q}(t)) + V \cdot \mathbb{E}\{\text{delay}(t) | \mathbf{Q}(t)\}) \quad (6)$$

Furthermore, according to **Theorem 1**, it is evident that the problem P1 can be converted into a computable one. Consequently, we can derive **Theorem 2**.

Theorem 2. Problem P1 can be equivalently transformed into Problem P2 through a reformulation that preserves the original objective and constraints as Eq.(7).

$$\mathbf{P2} : \min_{\delta\text{req}_k^{t,\text{in}}} \sum_{k=1}^N \left(v_k^{t,\text{dpp}} \right) \quad (7)$$

where

$$v_k^{t,\text{dpp}} = \underbrace{w_k Q_k(t) \cdot \delta\text{c}\bar{\text{p}}\text{u}_k^{t,\text{in}}}_{\text{stability}} + \underbrace{V \cdot \text{delay}_k^t \cdot \delta\text{req}_k^{t,\text{in}}}_{\text{performance}} \quad (8)$$

$v_k^{t,\text{dpp}}$ denotes the DPP value of node k , and delay_k^t represents the latency incurred when users connect to proxy node k both in time slot t .

Proof. See Appendix B. ■

In contrast to offline optimization problems, which typically demand comprehensive network information, the online approach to solving the optimization problem offers a more flexible and practical solution. It makes scheduling decisions by minimizing the total DPP, thereby achieving performance optimization while adhering to long-term stability constraints.

5.1.2 BPR Solutions for the Lyapunov Optimization

The **P2** problem can technically be solved; however, due to the non-linearity of \hat{f}_k , it becomes an **NP-hard** problem [56, 62], making it computationally expensive to obtain an exact solution. In practice, we employ a heuristic method known as the Big Process Rearrangement (BPR) [31] approach to obtain an approximation quickly. The algorithm prioritizes nodes with extreme values—either excessively high or abnormally low—to accelerate system convergence. This design aligns with empirical observations that a small number of anomalous nodes often dictate overall performance, either highly performant or severely degraded.

Algorithm 1 begins by proportionally allocating the total request increment $\delta \text{req}_k^{t,\text{in}}$ to all nodes based on their initial request rate at the beginning of slot t , $\text{req}_k^{t,\text{onset}}$ (line 1). Since this is a real-time scheduling system with second-level slots, the value of $\delta \text{req}_k^{t,\text{in}}$ is relatively small. The algorithm then computes $v_k^{t,\text{dpp}}$ for each node and identifies outliers using a median absolute deviation (MAD) threshold (lines 2–3). From lines 4–14, the process iteratively redistributes requests from extreme nodes to more stable ones to reduce the overall DPP. Nodes no longer performance-effective are deactivated and excluded from all subsequent scheduling logic. Finally, the adjusted per-node request changes are returned (line 15).

This heuristic enhances the global DPP by focusing on nodes with extreme $v_k^{t,\text{dpp}}$ values, redistributing requests to improve overall system acceleration performance and stability. Notably, the DPP consists of two components: the penalty term, which represents the accelerated performance metric, and the drift term, which reflects stability. When high $v_k^{t,\text{dpp}}$ values are driven by penalty (e.g., due to network latency), redistributing requests can mitigate the impact on system performance, potentially leading to a rapid convergence toward the minimum. However, when extreme $v_k^{t,\text{dpp}}$ values are caused by drift, they typically correspond to nodes with a large CPU cumulative deviation (LCCD) from the stability threshold, with the deviation either increasing rapidly (extremely high) or decreasing quickly (extremely low). In such cases, extremely high $v_k^{t,\text{dpp}}$ values can be rapidly flipped to extremely low ones—and vice versa—by a minor adjustment in the request rate, indicating a high degree of volatility. This highlights the need for prompt intervention to mitigate the destabilizing effects of nodes with LCCD. This suggests that nodes with LCCD are highly likely to significantly impact network stability, prompting us to take swift actions to offload

Algorithm 1: BPR for the Lyapunov Optimization

Input: Total request change $\delta \text{req}_k^{t,\text{in}}$ in slot t ;
proportion parameter p for redistribution step;
node set $k \in \mathcal{N}$

Output: Final per-node variation $\delta \text{req}_k^{t,\text{in}}$

- 1 **Init:** Assign $\delta \text{req}_k^{t,\text{in}}$ over \mathcal{N} by $\text{req}_k^{t,\text{onset}}$, and update $\{\text{req}_k^{t,\text{in}}\}_{k \in \mathcal{N}}$; // $\text{req}_k^{t,\text{in}} = \text{req}_k^{t,\text{onset}} + \delta \text{req}_k^{t,\text{in}}$
- 2 **Compute:** $\{v_k^{t,\text{dpp}}, \text{c}\bar{\text{p}}u_k^{t,\text{in}}\}_{k \in \mathcal{N}}$;
- 3 **Detect:** Identify outlier nodes O where $|v_k^{t,\text{dpp}} - \text{median}| > 3 \times \text{MAD}$, $S \leftarrow \emptyset$;
- 4 **while** $O \setminus S \neq \emptyset$ **do**
 - 5 $k^* = \arg \max_{k \in O \setminus S} |v_k^{t,\text{dpp}}|$
 - 6 Remove $p\%$ of $\text{req}_{k^*}^{t,\text{in}}$ as redistribution pool R ;
 - 7 Reassign R over $\mathcal{N} \setminus S$ by CPU $(1 - \text{c}\bar{\text{p}}u_k^{t,\text{in}}) \cdot C_k$;
update $\text{req}_k^{t,\text{in}}$; // $\mathcal{N} \setminus O$ non-singular set
 - 8 Update $\{v_k^{t,\text{dpp}}, \text{c}\bar{\text{p}}u_k^{t,\text{in}}\}_{k \in \mathcal{N}}$;
 - 9 **if** $\text{isImproved} \leftarrow \text{Check gains in } \sum_{k=1}^N v_k^{t,\text{dpp}}$ **then**
 - 10 | Update O with new $v_k^{t,\text{dpp}}$ and $3 \times \text{MAD}$;
 - 11 **else**
 - 12 | Revert, add k^* to S , and skip;
 - 13 **end**
 - 14 **end**
 - 15 **return:** Final $\delta \text{req}_k^{t,\text{in}} \leftarrow \text{req}_k^{t,\text{in}} - \text{req}_k^{t,\text{onset}}$;

their accumulated deviation.

5.2 Middle-Mile Scheduling

Middle-mile scheduling, which balances path acceleration and diversity, plays an integral role in maintaining system stability. It is essentially a constrained multi-path problem (CMPP), where the system filters out unstable nodes and selects K forwarding paths that satisfy both latency and convergence thresholds. During this process, the scheduling does not take into account its potential impact on node stability due to two primary considerations: first, proxy node capacity is enhanced through various proxying techniques and LinUCB-based tuning, mitigating stability concerns compared to the one-to-one user-to-proxy mapping in the last-mile. Second, the last-mile benefits from a flexible, responsive scheduling mechanism that quickly detects and recovers from node instability, reducing the need for such considerations in middle-mile scheduling.

5.2.1 Modelling as Maximum Flow with Conflicts

In this subsection, the CMPP problem is transformed into a maximum flow problem with conflicts (MFPC) formulation. Each non-source and non-sink node in the original network is modeled as a virtual edge. Specifically, a node k is repre-

sented as an edge $(i_k, j_k) \in A$, and the original edge $(k-1, k)$ is mapped to (j_{k-1}, i_k) . The capacity $u_{i_k j_k}$ and cost $l_{i_k j_k}$ of the edge correspond to the path admission limit and latency, respectively. The source node is assigned an input flow of K , representing the desired number of forwarding paths. By default, we set the capacity of original edges (e.g., u_{j_{k-1}, i_k}) to ∞ , while the capacity of virtual edges (i.e., $u_{i_k j_k}$) is set to K , enabling full path reuse unless otherwise restricted. The MFPC model is then formulated as Eq.(9):

$$\begin{aligned} & \max \mathcal{F} \quad (9) \\ \text{s.t.} \quad & \begin{cases} \sum_{(i,j) \in A} f_{ij} = \sum_{(j,i) \in A} f_{ji} \quad \forall i \in V \setminus \{s, t\} & (9.1) \\ f_{ij} \leq x_{ij} \theta_a u_{ij}, \quad \forall (i, j) \in A & (9.2) \\ x_{ij} \in \{0, 1\} & (9.3) \\ \max_{P \in \mathcal{P}} L(P) \leq \theta_L & (9.4) \end{cases} \end{aligned}$$

In Eq.(9), the objective is to maximize the overall flow \mathcal{F} across the network. The first constraint enforces flow conservation, ensuring that the inflow and outflow at each node are balanced as Eq.(9.1). The second constraint imposes an admission limit on each edge (i, j) , such that the flow does not exceed $\theta_a u_{ij}$, where $\theta_a \in [0, 1]$ is a configurable threshold controlling admissibility as Eq.(9.2). The third constraint is defined x_{ij} as a binary decision variable indicating whether an edge (i, j) is selected as Eq.(9.3). Additionally, the maximum path latency is bounded by θ_L as Eq.(9.4). Since MFPC is **NP-hard** [20], it cannot be solved by general maximum flow algorithms such as Ford–Fulkerson [42].

5.2.2 Carousel Greedy Approach for the MFPC

Algorithm 2 initializes the path set S and residual network G_f , then iteratively selects feasible paths P from s to t , adds them to S , and updates the flow. Once no more paths are found, each $P \in S$ is added to the global set \mathcal{P} with frequency $\tau_P = 1$. The initial solution is stored as S^* with objective value z^* (lines 1–4). The Carousel process then begins by removing the most recently selected $\beta \cdot |S|$ paths from S , followed by $\alpha \cdot |S|$ iterations to search for an improved solution (lines 5–6). In each iteration, the oldest path is removed, and the most

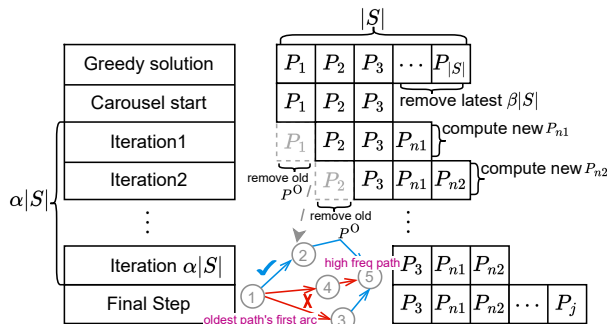


Fig. 8. The Logic Diagram of the Carousel Greedy.

Algorithm 2: Carousel Greedy for the MFPC

Input: Original graph $G = (V, A)$; source node s ; sink node t ; α and β parameters.

Output: Solution S^* .

```

1 Init:  $S \leftarrow \langle \rangle$ ;  $G_f \leftarrow$  residual graph of  $G$ ;
2 Greedily select  $P (s \rightarrow t)$  satisfying admission and
  latency; add to  $S$ , update flow and  $G_f$  until done;
3  $\mathcal{P} \leftarrow \{P : P \in S\}$ ;  $\tau_P \leftarrow 1, \forall P \in S$ ;
4  $S^* \leftarrow S$ ;  $z^* \leftarrow z(S)$ ;
5  $S^C \leftarrow$  Remove the  $\beta \cdot |S|$  newly selected paths from  $S$ ;
6 for  $k \in \{1, \dots, \alpha \cdot |S|\}$  do
7   Remove the oldest path  $P^O$  from  $S^C$ ;
8   Update the residual network  $G_f$ ;
9   Set  $\tau_{\max} \leftarrow \max_{P \in \mathcal{P}} \tau_P$ ; // highest freq
10  Let  $P_{\tau_{\max}}$  be the oldest path with frequency  $\tau_{\max}$ ;
11  Zero residuals on first arc of  $P^O$  and all of  $P_{\tau_{\max}}$ ;
12  Find  $P$  in  $G_f$  s.t. admission & latency hold;
13  while  $P$  is not empty do
14     $\mathcal{P} \leftarrow \mathcal{P} \cup P$ ;  $\tau_P \leftarrow \tau_P + 1$ ;
15    Add  $P$  to  $S^C$ , compute the flow increment for
      path  $P$ , and update the residual network  $G_f$ ;
16    Find path  $P$  in  $G_f$  satisfies both admission
      limit and latency constraints;
17  end
18  If  $z^* \leq z(S^O)$  then  $S^* \leftarrow S^O$ ;  $z^* \leftarrow z(S^C)$ ;
19 end
20 return: Solution  $S^*$ 

```

frequently selected path is identified, with ties broken by preferring earlier-generated candidates (lines 7–10). To promote path diversity, the first arc of the oldest path and all arcs of the most frequent path $P_{\tau_{\max}}$ are banned in the residual graph. A new feasible path P is then searched (lines 11–12). If P is non-empty, the algorithm continues to search for additional valid paths under the updated constraints (lines 13–17). If the objective value improves, the best solution S^* and its value z^* are updated (line 18). After all iterations, the optimal solution S^* is returned (line 20). The overall logic is illustrated in Fig. 8.

The Carousel Greedy algorithm balances optimality and efficiency by iteratively selecting paths that satisfy conflict constraints and adjusting network flow. It prioritizes high-frequency paths based on the residual network state, ensuring efficient resource use and strong solution quality. This approach quickly approximates optimal solutions, ideal for large-scale problems where exact solutions are impractical.

6 Resilience Pillars

Backup Paths & Fast Recovery. Backup paths and fast recovery are the most fundamental aspects of network stability. In the event of a network failure during the information for-

warding process, the proxy node will redirect traffic to the target destination via a backup path, notify ingress node in the reverse direction of the forwarding path to reroute, and simultaneously inform the controllers about the event. This mechanism enables seamless recovery and second-level rerouting. For instance, a relay node R computes backup paths to a target region D , deliberately avoiding next-hop nodes burdened with substantial traffic to D . Node groups that serve different areas can inherently carry out the cross-backup operations mentioned above. This is a result of time-zone differences between regions, which aligns with common intuition.

Horizontal Scaling. The DPP algorithm guides scheduling decisions by quantitatively balancing drift (i.e., stability queue backlog) and penalty (i.e., path delay). This trade-off helps optimize long-term system acceleration performance and stability. But, when a new node is added horizontally to the system, it typically has a lighter load and therefore a lower $v_k^{t, \text{dpp}}$ value. This often leads to a rapid surge of incoming requests within a short period of time, causing a sharp increase in its queue backlog and severely impacting overall system stability. To address this issue, the place-holder backlog technique [57] is introduced. By initializing the mean queue backlog to a non-zero value $Q_k(0) = Q_k^{\text{place}}$, the system can reduce the rate of backlog growth and maintain stable performance for newly added nodes.

7 Evaluations

7.1 System Building and Experiment Setup

For network provisioning, the experimental scenario is designed to support a million-level accelerated RPS. We partition the world into seven regions and procure resources from cloud vendors of varying tiers, including Vultr, DigitalOcean, GCP, and AWS. The resource procurement adheres to the following principles: In the last-mile, we endeavor to enhance the coverage density by using a large number of low-spec resources. In the middle-mile, we select fewer high-performance VMs to strengthen the stability and deploy them at key subsea cable network hubs [68], such as Singapore, Frankfurt, New York, and Los Angeles, aligning the network with the global communication backbone to improve connectivity and reliability. Following these principles, as shown in Fig. 9, we have provisioned 50 VMs across diverse regions and cloud providers worldwide. The VMs span configurations from 4C8G to 16C32G, 80% of which are provisioned as 8C16G, primarily because this configuration offers a favorable trade-off between performance and resource coverage.

Regarding deployment, on the data plane, proxy nodes in different regions are networked through *etcd* to synchronously update the basic information within the group in real-time. The master node is responsible for assigning scheduling tasks, and the proxy master node is, by default, in charge of the last-mile routing calculation. On the control plane, two control units are set up. Each control unit consists of a controller and

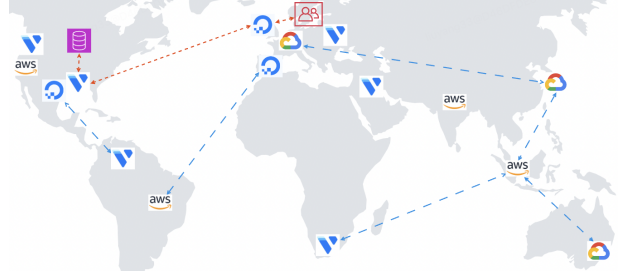


Fig. 9. *Arcturus* Global Multi-Cloud Deployment Overview.

a storage component, and they are deployed in New York and Singapore, respectively. Proxy nodes will communicate with the nearest controller, and the controllers synchronize global data in real-time via the *etcd* network. It should be emphasized that the underlying communication of the *etcd* service also utilizes *Arcturus*'s own acceleration service to enhance predictability and timeliness.

In terms of access, users use Layer-7 routing to access the network. Each region is configured with a *Traefik* [9] service featuring the HTTP 302 redirect function. Every 5s, users obtain the access list and weight information from this service and access the network according to the strategy.

7.2 Acceleration Performance Surpasses

Evaluating *Arcturus* Over the Public Internet. As shown in Fig. 10a, to assess *Arcturus*'s performance over the public Internet, we deployed servers in Washington, D.C., London, and Osaka, respectively. Requests were sent from multiple regions worldwide to these locations, routed through both *Arcturus* and the public Internet for comparison. The results demonstrate that *Arcturus* achieves approximately a 50% latency improvement over the public Internet on average across global access points. This performance gain is primarily attributed to three factors. First, the proxy network reduces routing lookup overhead and shortens route convergence time, leading to lower latency. Second, cloud data centers generally offer higher network quality and more stable backbone links. Third, *Arcturus* detours through intermediate relay nodes, bypassing congested or inefficient paths, as demonstrated by traffic from Johannesburg to Sydney benefiting from a 20% latency reduction when relayed through Singapore.

Comparing *Arcturus* with Commercial GAs. Fig. 10b and 10c compare the performance of *Arcturus* with commercial GA services. Theoretically, commercial GAs, which require server deployment within provider-managed infrastructure, should deliver superior first-mile performance, which may help reduce overall end-to-end latency. Nevertheless, as shown in Fig. 10b, *Arcturus* consistently outperforms GCP Global Load Balancing by up to 40%, especially in regions with poorer connectivity such as the Middle East and the Southern Hemisphere. This improvement may be attributed to GCP's sparse Point of Presence (POP) coverage in these

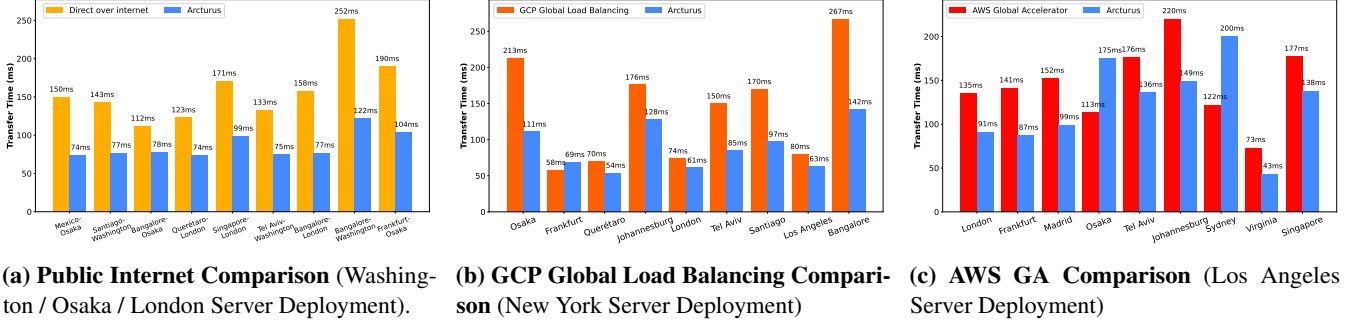


Fig. 10. (a) Direct vs. *Arcturus*; (b, c) *Arcturus* vs. commercial GA services.

developing areas. Fig. 10c also shows that *Arcturus* generally surpasses AWS Global Accelerator by around 35%. While this per-request improvement may seem modest, at a scale of millions of RPS it translates into substantial aggregate latency savings and throughput gains. In some regions (e.g., Australia), where network quality is generally poor but strategically important, AWS outshines *Arcturus*, likely due to its use of dedicated backbone links in such critical areas. Conversely, *Arcturus* achieves superior performance in Europe and North America by deploying numerous low-cost, high-density edge nodes, effectively reducing last-mile access latency. In our measurements, GCP’s performance and stability appeared inferior to those of AWS. This may be attributed to differences in service pricing, as GCP charges \$0.01 per GB [34], whereas AWS is priced at \$0.035 per GB. For example, in a test case from Singapore to Washington, D.C., latency via GCP occasionally reached up to 0.5s.

7.3 Proxy Nodes with Exceptional Efficiency

Evaluating Proxy Performance Under High Load. To assess the throughput limits of proxy nodes and obtain an initial piecewise approximation of \hat{f}_k , we conducted stress tests on typical VM configurations (e.g., 4C8G, 8C16G, and 16C32G). In each 5-second slot, we injected randomized request increments δreq ranging from 100 to 300 to emulate realistic user request fluctuations. This range was chosen to reflect typical per-slot variations given the short time granularity. Experimental results show that proxy nodes can remain stable and sustain traffic without degradation up to 80% CPU utilization. Beyond this point, we fitted \hat{f}_k for CPU utilization levels within the 60–70% and 70–80% bands. Figure 11 illustrates the results for the 8C16G VM (shared CPU, Vultr LA)⁴. The maximum RPS capacity reached approximately 25,000, indicating that 50 such VMs can collectively serve over one million RPS. The piecewise linear relationship between request increments and CPU utilization increments δcpu is given by $\delta\text{cpu} = 340 \times \delta\text{req} - 1300$ for $\text{cpu} \in [60\%, 70\%]$,

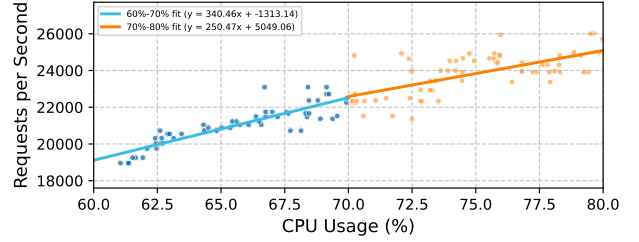


Fig. 11. Proxy RPS Benchmark and \hat{f}_k Fitting on 8C16G VM.

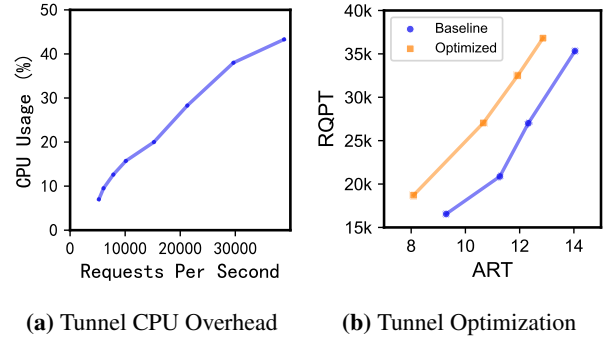


Fig. 12. Tunnel Benchmark between 8C16G VMs.

and $\delta\text{cpu} = 250 \times \delta\text{req} + 5000$ for $\text{cpu} \in (70\%, 80\%]$.

Enhancing Overlay Tunnel Performance. *Arcturus* leverages three key techniques—TCP connection pooling, stream multiplexing, and packet merging—to optimize connection management, thereby improving forwarding efficiency and minimizing computation overhead. As shown in Fig. 12a, we evaluated the tunnel performance between two 8C16G VMs (shared-CPU, Vultr, Los Angeles). The results show that even when forwarding 20,000 RPS, the system only consumed approximately 20% CPU without degrading average request processing time. This also supports our design principle of differentiating last-mile and middle-mile scheduling strategies: the middle-mile is not responsible for node stability, since the efficient forwarding logic ensures that its adjustments have minimal impact on overall CPU load. Building on this, Fig. 12b illustrates how the reinforcement learning

⁴VMs differ slightly across providers and regions, but those with the same configuration show consistent trends; we showcase one representative example, similarly hereafter.

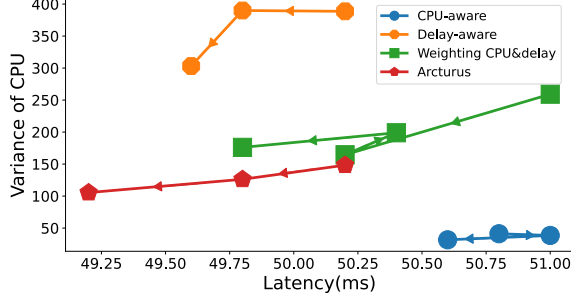


Fig. 13. Performance Implications of Last-Mile Scheduling.

algorithm dynamically adjusts the tunnel parameters. The plot clearly shows that these adjustments effectively increase tunnel throughput, measured by the number of requests processed per unit time, while simultaneously reducing the average request processing time.

7.4 Efficient and Precise Routing Strategies

Last-Mile Traffic Steering. We schedule last-mile traffic by minimizing a global DPP objective, where system stability is defined as the product of the cumulative backlog exceeding a threshold and the acceleration of deviation. This formulation extends beyond reactive, greedy heuristics, maintaining a more effective long-term balance between stability and latency. We compare against dynamic balancing baselines: latency-aware, CPU-aware, and joint strategies. In practical experiments, we place the load generator in Dallas and target the US West proxy group (10 \times 8C16G VMs) to amplify RTT variation intentionally. As shown in Fig. 13, *Arcturus* consistently maintains a superior dynamic trade-off between global stability—indicated by lower CPU variance across group nodes—and acceleration performance, outperforming existing methods.

Due to regional limitations, the number of proxy nodes in a region is generally not large. In our simulations, with up to 50 nodes, the scheduling algorithm converges within 100ms. Regarding the redistribution ratio p , when node capacities are similar we set $p = \frac{1}{2}$; if capacities vary significantly, we select p from the descending series $\{\frac{1}{2}, \frac{1}{4}, \frac{1}{8}, \dots\}$ to perform rapid, adaptive reallocation.

Mid-Mile Routing Optimization. Under a fixed latency constraint and a bounded path reuse rate, *Arcturus* seeks a Pareto frontier that balances path count and diversity to improve system stability through path diversification. We compare this with LiveNet [47] and ONEWAN [43]. LiveNet uses a K -Shortest [28] paths algorithm and selects final routes based on diversity heuristics, emphasizing path uniqueness. ONEWAN follows a solver chaining approach, first computing a candidate set via a maximum-flow formulation, then applying diversity-based selection. While both emphasize diverse routing, LiveNet favors diversity, whereas ONEWAN prioritizes the number of viable paths. As shown in Fig. 14 and Tab. 2, we

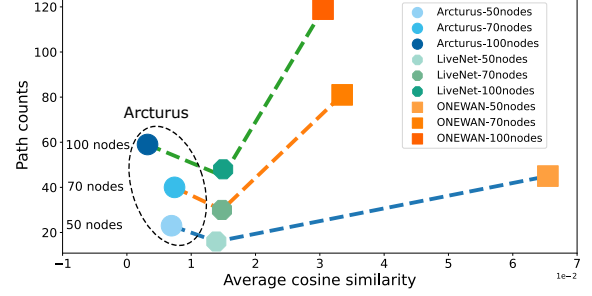


Fig. 14. Evaluating Middle-Mile Scheduling Strategies.

Table 2: Best Solution Using Grid Search

Nodes	α	β	PathCnt	CosSim	Time (ms)
50	2	70%	23	6.9E-3	62
70	2	70%	40	7.4E-4	274
100	1	80%	59	3.2E-4	642

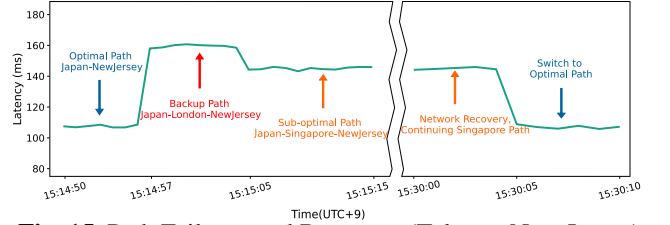


Fig. 15. Path Failover and Recovery (Tokyo→New Jersey).

conducted experiments at node scales of 50 (real deployment), 70, and 100 to evaluate *Arcturus*’s routing algorithm (with arc density d fixed at 0.4 in all cases.). The results demonstrate that, with average path latency being similar, *Arcturus*’s multi-objective optimization approach discovers the Pareto frontier between path count and path diversity, significantly outperforming both LiveNet and ONEWAN. Furthermore, the computation completes in roughly 600 ms⁵ for the 100-node network, comfortably within the 5-second cycle limit.

7.5 Stable and Reliable Operation Assurance

Case Study 1: Network Issues at GCP-Tokyo. We present a case study demonstrating *Arcturus*’s backup path and failure recovery mechanism in response to a transient network issue. As shown in Fig. 15, at 15:14:54, the GCP-Tokyo node experienced outbound network degradation, resulting in latency spikes on direct paths from Tokyo to New Jersey (Fig. 18). The GCP-Tokyo node promptly activated a backup route via Europe and simultaneously initiated a recalculation of the global optimal path. By 15:14:57, all traffic had been rerouted through Tokyo→London→New Jersey. Eight seconds later, at 15:15:05, the system dynamically transitioned to a new, better-performing route: Tokyo→Singapore→New Jersey. Approximately 15 minutes later, once Tokyo’s network conditions

⁵By applying grid search along with early pruning techniques, the solving time can be reduced to 100–300ms.

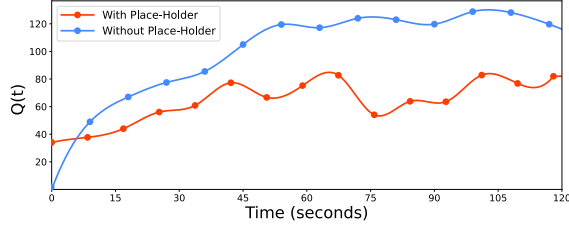


Fig. 16. Stabilizing VM Addition with Place-Holder.

stabilized, traffic automatically reverted to the original optimal path—showcasing *Arcturus*’s rapid failover and real-time recovery capabilities.

Case Study 2: Adding a VM to the Proxy Group. We introduce the place-holder technique to enhance the system’s responsiveness under low queue backlogs. This approach sets a non-zero initial value for the virtual queue in the DPP algorithm, $Q_k(0) = Q_k^{\text{place}}$, thereby simulating a higher perceived load than the actual one. By ensuring the perceived load exceeds the actual load, the scheduling strategy can intervene earlier and prevent excessive queue growth when a new node joins the proxy group, mitigating scheduling delays in low-backlog scenarios. As illustrated in Fig. 16, when the overall CPU utilization of the U.S. West proxy group reaches around 60%, an AWS-California node is added to relieve system pressure. Its $Q_k(0)$ is set to the median value of the queue log from the proxy group nodes, effectively reducing queue accumulation and fluctuations. This approach achieves lower latency and improved stability while preserving the algorithm’s optimization effectiveness.

7.6 Cost-effectiveness Advantage Highlights

Pricing Benefits. The pricing structure of mainstream commercial GA services typically consists of two components: operational fees and data transfer charges. GCP tends to have higher operational overhead, while AWS incurs significantly higher bandwidth costs. These pricing differences reflect distinct operational strategies and the fallback-oriented usage pattern of many customers. In practice, users often configure acceleration services as a backup and only route traffic through them during performance degradation on the public internet. As a result, many registered users do not generate significant traffic despite having rules in place.

Arcturus, by contrast, primarily builds its infrastructure using VMs from tier-2/3 cloud providers. A typical 8C16G instance costs approximately \$0.132 per hour, meaning that a 50-node deployment requires just \$6.6 per hour in compute costs. Average bandwidth cost is below \$0.01 per GB, which allows *Arcturus* to reduce total costs by up to 71% compared to AWS when handling millions of RPS in a single-tenant deployment. When operated as a public acceleration platform—a deployment model we favor—*Arcturus* requires operation charges from fewer than 300 registered users to cover daily infrastructure costs, after which the platform be-

comes profitable through bandwidth and operational margins.

8 Related Work

(i)Overlay Network. Overlay networks enhance the performance, stability, and functionality of the underlying network without altering its core architecture. Early systems like RON [16] provided resilient forwarding as a fallback to improve stability. With the rise of applications such as TikTok [8], overlay networks have evolved to support diverse use cases including RTC [26], video conferencing [51, 75], distributed computation [44], and P2P systems [73, 80]. Modern overlays now emphasize not only functionality but also performance, robustness, and cost efficiency.

(ii)Elastic Cloud Overlay Network. Cloud resources offer cost-efficiency, reliability, and scalability, making them increasingly popular in network systems. XRON [75] adopts a hybrid approach to balance performance and cost, while Sky-plane [39] and Cloudcast [74] build full cloud-based overlay networks for efficient inter-datacenter data transfer. Recent work [76, 79] further proposes general scheduling strategies across heterogeneous instances (e.g., on-demand vs. spot) to optimize the trade-off between availability and cost in cloud overlay networks.

(iii)Network Scheduling. Network scheduling efficiently manages network resources and traffic to optimize data transmission, improve performance, and ensure fairness [46, 48, 49]. Often reducible to NP-hard problems like the multi-commodity flow problem [30], exact solutions are computationally challenging. Due to resource constraints and time limitations, approximate strategies [43, 47, 75], stochastic optimization [61, 65, 66], or deep learning techniques [12, 37] are used to approach the optimal solution. However, due to performance and stability limitations of cloud resources, these solutions may not apply directly to *Arcturus*. Moreover, effective network scheduling requires not only algorithms but also flexible models [10, 11], user behavior insights [29, 40, 50, 63], and frameworks built on federated learning [23, 52] or edge cloud resources [53, 64] for enhanced accuracy and reliability.

9 Conclusion

This paper presents *Arcturus*, a cloud-native GA system that addresses the limitations of commercial GA services in cost, flexibility, and global coverage. *Arcturus* dynamically composes a multi-cloud proxy network and coordinates it through a high-capacity data plane and an intelligent scheduling control plane, effectively handling heterogeneous and dynamic workloads. Under millions of RPS, it outperforms commercial GA services by up to 1.7× in acceleration performance and reduces cost by 71%, while maintaining over 80% resource efficiency. Moving forward, we plan to extend *Arcturus* toward a unified platform for both GA and bulk data transfer, and explore more autonomous, demand-aware proxy network composition to support evolving traffic and deployment needs.

References

- [1] Coursera. <https://www.coursera.org/>, Accessed:2025-04-20.
- [2] Envoy. <https://www.envoyproxy.io/>, Accessed:2025-04-20.
- [3] Etc. <https://etc.io/>, Accessed:2025-04-20.
- [4] Haproxy. <https://www.haproxy.org/>, Accessed:2025-04-20.
- [5] Nginx. <https://nginx.org/>, Accessed:2025-04-20.
- [6] Segment-routing. <https://www.segment-routing.net/>, Accessed:2025-04-20.
- [7] Smux. <https://github.com/xtaci/smux>, Accessed:2025-04-20.
- [8] Tiktok. <https://www.tiktok.com/>, Accessed:2025-04-20.
- [9] Traefik. <https://traefik.io/traefik/>, Accessed:2025-04-20.
- [10] Satyajeet Singh Ahuja, Vinayak Dangui, Kirtesh Patil, Manikandan Somasundaram, Varun Gupta, Mario Sanchez, Guanqing Yan, Max Noormohammadpour, Alaleh Razmjoo, Grace Smith, Hao Zhong, Abhinav Triguna, Soshant Bali, Yuxiang Xiang, Yilun Chen, Prabhakaran Ganesan, Mikel Jimenez Fernandez, Petr Lapukhov, Guyue Liu, and Ying Zhang. Network entitlement: contract-based network sharing with agility and slo guarantees. In Proceedings of the ACM SIGCOMM Conference, pages 250–263, New York, NY, USA, 2022.
- [11] Satyajeet Singh Ahuja, Varun Gupta, Vinayak Dangui, Soshant Bali, Abishek Gopalan, Hao Zhong, Petr Lapukhov, Yiting Xia, and Ying Zhang. Capacity-efficient and uncertainty-resilient backbone network planning with hose. In Proceedings of the ACM SIGCOMM Conference, page 547–559, New York, NY, USA, 2021.
- [12] Abd AlRhman AlQiam, Yuanjun Yao, Zhaodong Wang, Satyajeet Singh Ahuja, Ying Zhang, Sanjay G. Rao, Bruno Ribeiro, and Mohit Tawarmalani. Transferable neural wan te for changing topologies. In Proceedings of the ACM SIGCOMM Conference, pages 86–102, New York, NY, USA, 2024. Association for Computing Machinery.
- [13] Amazon Web Services. Global accelerator. https://aws.amazon.com/global-accelerator/?nc1=h_ls, Accessed:2025-04-20.
- [14] Amazon Web Services. Amazon ec2. <https://aws.amazon.com/ec2/>, Accessed:2025-04-24.
- [15] Amazon Web Services. Global accelerator pricing. <https://aws.amazon.com/global-accelerator/pricing/>, Accessed:2025-04-24.
- [16] David Andersen, Hari Balakrishnan, Frans Kaashoek, and Robert Morris. Resilient overlay networks. ACM SIGOPS Operating Systems Review, 2001.
- [17] L Andersson, I Minei, and B Thomas. Rfc 5036: Ldp specification, 2007.
- [18] Vaibhav Bajpai, Steffie Jacob Eravuchira, and Jürgen Schönwälder. Dissecting last-mile latency characteristics. ACM SIGCOMM Computer Communication Review, 47(5):25–34, 2017.
- [19] Kamal Benzekki, Abdeslam El Fergougui, and Abdelbaki Elbelrhiti Elalaoui. Software-defined networking (sdn): a survey. Security and communication networks, 9(18):5803–5833, 2016.
- [20] F Carrabs, R Cerulli, R Mansini, D Serra, and C Sorgente. Hybridizing carousel greedy and kernel search: A new approach for the maximum flow problem with conflict constraints. European Journal of Operational Research, 2025.
- [21] Ruobing Chen, Haosen Shi, Yusen Li, Xiaoguang Liu, and Gang Wang. Olpart: Online learning based resource partitioning for colocating multiple latency-critical jobs on commodity computers. In Proceedings of the Eighteenth European Conference on Computer Systems, pages 347–364, 2023.
- [22] Yingying Chen, Sourabh Jain, Vijay Kumar Adhikari, and Zhi-Li Zhang. Characterizing roles of front-end servers in end-to-end performance of dynamic content distribution. In ACM SIGCOMM conference on Internet measurement conference, pages 559–568, 2011.
- [23] Cheng-Wei Ching, Xin Chen, Taehwan Kim, Bo Ji, Qingyang Wang, Dilma Da Silva, and Liting Hu. Totoro: A scalable federated learning engine for the edge. In Proceedings of the Nineteenth European Conference on Computer Systems, pages 182–199, New York, NY, USA, 2024.
- [24] Cloudflare. Argo-smart-routing. <https://developers.cloudflare.com/argo-smart-routing/>, Accessed:2025-04-20.
- [25] Cloudflare. Spectrum. <https://developers.cloudflare.com/spectrum/>, Accessed:2025-04-20.
- [26] Sandesh Dhawaskar Sathyanarayana, Kyunghan Lee, Dirk Grunwald, and Sangtae Ha. Converge: Qoe-driven multipath video conferencing over webrtc. In

Proceedings of the ACM SIGCOMM 2023 Conference, pages 637–653, New York, NY, USA, 2023.

- [27] DigitalOcean. Droplets. <https://cloud.digitalocean.com/droplets?i=8f55d5>, Accessed:2025-04-20.
- [28] David Eppstein. Finding the k shortest paths. *SIAM Journal on computing*, 28(2):652–673, 1998.
- [29] Andrew D. Ferguson, Steve Gribble, Chi-Yao Hong, Charles Killian, Waqar Mohsin, Henrik Muehe, Joon Ong, Leon Poutievski, Arjun Singh, Lorenzo Vicisano, Richard Alimi, Shawn Shuoshuo Chen, Mike Conley, Subhasree Mandal, Karthik Nagaraj, Kondapa Naidu Bollineni, Amr Sabaa, Shidong Zhang, Min Zhu, and Amin Vahdat. Orion: Google’s Software-Defined networking control plane. In *18th USENIX Symposium on Networked Systems Design and Implementation*, pages 83–98, April 2021.
- [30] L.K. Fleischer. Approximating fractional multicommodity flow independent of the number of commodities. In *40th Annual Symposium on Foundations of Computer Science (Cat. No.99CB37039)*, pages 24–31, 1999.
- [31] Haris Gavranović and Mirsad Buljubašić. An efficient local search with noising strategy for google machine reassignment problem. *Annals of Operations Research*, 242:19–31, 2016.
- [32] Bolaji Gbadamosi, Luigi Leonardi, Tobias Pulls, Toke Høiland-Jørgensen, Simone Ferlin-Reiter, Simo Sorce, and Anna Brunström. The ebpf runtime in the linux kernel. *ArXiv*, abs/2410.00026, 2024.
- [33] GCP. Load-balancing. <https://cloud.google.com/load-balancing>, Accessed:2025-04-20.
- [34] GCP. Global load balancing pricing. <https://cloud.google.com/vpc/network-pricing/>, Accessed:2025-04-24.
- [35] GE Gevernova. Integrated electrical propulsion system for us navy ddg 1000 destroyers. <https://www.gevernova.com/power-conversion/case-study/integrated-electrical-propulsion-system-for/-us-navy-ddg-1000-destroyers>, Accessed:2025-04-24.
- [36] Google Cloud Platform. Vm instances. <https://console.cloud.google.com/compute/instances>, Accessed:2025-04-20.
- [37] Fei Gui, Songtao Wang, Dan Li, Li Chen, Kaihui Gao, Congcong Min, and Yi Wang. Redte: Mitigating subsecond traffic bursts with real-time and distributed traffic engineering. In *Proceedings of the ACM SIGCOMM Conference*, pages 71–85, New York, NY, USA, 2024.
- [38] Gongde Guo, Hui Wang, David Bell, Yaxin Bi, and Kieran Greer. Knn model-based approach in classification. In *On The Move to Meaningful Internet Systems 2003: CoopIS, DOA, and ODBASE: OTM Confederated International Conferences, CoopIS, DOA, and ODBASE 2003, Catania, Sicily, Italy, November 3-7, 2003. Proceedings*, pages 986–996. Springer, 2003.
- [39] Paras Jain, Sam Kumar, Sarah Wooders, Shishir G. Patil, Joseph E. Gonzalez, and Ion Stoica. Skyplane: Optimizing transfer cost and throughput using Cloud-Aware overlays. In *20th USENIX Symposium on Networked Systems Design and Implementation*, pages 1375–1389, Boston, MA, April 2023.
- [40] Saurabh Jha, Archit Patke, Jim Brandt, Ann Gentile, Benjamin Lim, Mike Showerman, Greg Bauer, Larry Kaplan, Zbigniew Kalbarczyk, William Kramer, and Ravi Iyer. Measuring congestion in High-Performance datacenter interconnects. In *17th USENIX Symposium on Networked Systems Design and Implementation (NSDI 20)*, pages 37–57, Santa Clara, CA, February 2020.
- [41] Shanmukh Sai Kataru, Rohith Gude, Shoaib Shaik, Lalithesh VNSS Sathvik Kota, Balajee RM, et al. Cost optimizing cloud based docker application deployment with cloudfront and global accelerator in aws cloud. In *2023 International Conference on Sustainable Communication Networks and Application (ICSCNA)*, pages 200–208. IEEE, 2023.
- [42] Jon Kleinberg and Eva Tardos. *Algorithm design*. Pearson Education India, 2006.
- [43] Umesh Krishnaswamy, Rachee Singh, Paul Mattes, Paul-Andre C Bissonnette, Nikolaj Bjørner, Zahira Nasrin, Sonal Kothari, Prabhakar Reddy, John Abeln, Srikanth Kandula, Himanshu Raj, Luis Irun-Briz, Jamie Gaudette, and Erica Lan. OneWAN is better than two: Unifying a split WAN architecture. In *20th USENIX Symposium on Networked Systems Design and Implementation*, pages 515–529, Boston, MA, April 2023.
- [44] Dhruv Kumar, Sohaib Ahmad, Abhishek Chandra, and Ramesh K. Sitaraman. Aggnet: Cost-aware aggregation networks for geo-distributed streaming analytics. In *IEEE/ACM Symposium on Edge Computing (SEC)*, pages 297–311, 2021.
- [45] Adam Langley, Alistair Riddoch, Alyssa Wilk, Antonio Vicente, Charles Krasnic, Dan Zhang, Fan Yang, Fedor Kouranov, Ian Swett, Janardhan Iyengar, Jeff Bailey, Jeremy Dorfman, Jim Roskind, Joanna Kulik, Patrik Westin, Raman Tenneti, Robbie Shade, Ryan Hamilton, Victor Vasiliev, Wan-Teh Chang, and Zhongyi Shi.

The quic transport protocol: Design and internet-scale deployment. In Proceedings of the Conference of the ACM Special Interest Group on Data Communication, pages 183–196, New York, NY, USA, 2017. Association for Computing Machinery.

- [46] Jialong Li, Haotian Gong, Federico De Marchi, Aoyu Gong, Yiming Lei, Wei Bai, and Yiting Xia. Uniform-cost multi-path routing for reconfigurable data center networks. In Proceedings of the ACM SIGCOMM Conference, pages 433–448, New York, NY, USA, 2024.
- [47] Jinyang Li, Zhenyu Li, Ri Lu, Kai Xiao, Songlin Li, Jufeng Chen, Jingyu Yang, Chunli Zong, Aiyun Chen, Qinghua Wu, Chen Sun, Gareth Tyson, and Hongqiang Harry Liu. Livenet: a low-latency video transport network for large-scale live streaming. pages 812–825, 2022.
- [48] Junru Li, Youyou Lu, Qing Wang, Jiazhen Lin, Zhe Yang, and Jiwu Shu. AINiCo: SmartNIC-accelerated contention-aware request scheduling for transaction processing. In USENIX Annual Technical Conference (USENIX ATC), pages 951–966, Carlsbad, CA, July 2022.
- [49] Xing Li, Xiaochong Jiang, Ye Yang, Lilong Chen, Yi Wang, Chao Wang, Chao Xu, Yilong Lv, Bowen Yang, Taotao Wu, Haifeng Gao, Zikang Chen, Yisong Qiao, Hongwei Ding, Yijian Dong, Hang Yang, Jianming Song, Jianyuan Lu, Pengyu Zhang, Chengkun Wei, Zihui Zhang, Wenzhi Chen, Qinming He, and Shunmin Zhu. Triton: A flexible hardware offloading architecture for accelerating apsara vswitch in alibaba cloud. In Proceedings of the ACM SIGCOMM 2024 Conference, ACM SIGCOMM ’24, pages 750–763, New York, NY, USA, 2024. Association for Computing Machinery.
- [50] Zhenyu Li, Jinyang Li, Qinghua Wu, Gareth Tyson, and Gaogang Xie. A large-scale measurement and optimization of mobile live streaming services. IEEE Transactions on Mobile Computing, 22(12):7294–7309, 2023.
- [51] Xianshang Lin, Yunfei Ma, Junshao Zhang, Yao Cui, Jing Li, Shi Bai, Ziyue Zhang, Dennis Cai, Hongqiang Harry Liu, and Ming Zhang. Gso-simulcast: global stream orchestration in simulcast video conferencing systems. In Proceedings of the ACM SIGCOMM Conference, pages 826–839, New York, NY, USA, 2022.
- [52] Juncal Liu, Jessie Hui Wang, and Yimin Jiang. Janus: A unified distributed training framework for sparse mixture-of-experts models. In Proceedings of the ACM SIGCOMM Conference, pages 486–498, New York, NY, USA, 2023. Association for Computing Machinery.
- [53] Congcong Miao, Zhizhen Zhong, Yunming Xiao, Feng Yang, Senkuo Zhang, Yinan Jiang, Zizhuo Bai, Chaodong Lu, Jingyi Geng, Zekun He, Yachen Wang, Xianneng Zou, and Chuanchuan Yang. Megate: Extending wan traffic engineering to millions of endpoints in virtualized cloud. In Proceedings of the ACM SIGCOMM Conference, pages 103–116, New York, NY, USA, 2024.
- [54] Microsoft. Microsoft-365. <https://www.microsoft.com/en-sg/microsoft-365/mobile>, Accessed:2025-04-20.
- [55] Microsoft Azure. Virtual machines. <https://portal.azure.com/#browse/Microsoft.Compute%2FVirtualMachines>, Accessed:2025-04-20.
- [56] Michael Neely. Stochastic network optimization with application to communication and queueing systems. Morgan & Claypool Publishers, 2010.
- [57] Michael J Neely and Rahul Ugaonkar. Opportunism, backpressure, and stochastic optimization with the wireless broadcast advantage. In 2008 42nd Asilomar Conference on Signals, Systems and Computers, pages 2152–2158. IEEE, 2008.
- [58] Erik Nygren, Ramesh K. Sitaraman, and Jennifer Sun. The akamai network: a platform for high-performance internet applications. ACM SIGOPS Operating Systems Review, 44:2–19, 2010.
- [59] Abhinav Pathak, Y. Angela Wang, Cheng Huang, Albert Greenberg, Y. Charlie Hu, Randy Kern, Jin Li, and Keith W. Ross. Measuring and evaluating tcp splitting for cloud services. In Passive and Active Measurement, pages 41–50, Berlin, Heidelberg, 2010.
- [60] Mohammad Azmi Ridwan, Nurul Asyikin Mohamed Radzi, Wan Siti Halimatul Munirah Wan Ahmad, Fairuz Abdullah, Md Zaini Jamaludin, and Mohd Nasim Zakaria. Recent trends in mpls networks: technologies, applications and challenges. IET Communications, 14(2):177–185, 2020.
- [61] Utsav Sadana, Abhilash Chenreddy, Erick Delage, Alexandre Forel, Emma Frejinger, and Thibaut Vidal. A survey of contextual optimization methods for decision-making under uncertainty. European Journal of Operational Research, 320(2):271–289, 2025.
- [62] Mohamed Sana, Mattia Merluzzi, Nicola di Pietro, and Emilio Calvanese Strinati. Energy efficient edge computing: When lyapunov meets distributed reinforcement learning. In 2021 IEEE International Conference on Communications Workshops (ICC Workshops), pages 1–6, 2021.

- [63] Brandon Schlinker, Italo Cunha, Yi Ching Chiu, Srikanth Sundaresan, and Ethan Katz-Bassett. Internet performance from facebook’s edge. 2019.
- [64] Brandon Carl Schlinker, Hyojeong Kim, Timothy Cui, Ethan B Katz-Bassett, Harsha V Madhyastha, xcd, Talo S Cunha, James Quinn, Saif Hasan, and Petr Lapukhov. Engineering egress with edge fabric: Steering oceans of content to the world. 2017.
- [65] Karmel S Shehadeh and Rema Padman. A distributionally robust optimization approach for stochastic elective surgery scheduling with limited intensive care unit capacity. *European Journal of Operational Research*, 290(3):901–913, 2021.
- [66] Karmel S. Shehadeh and Rema Padman. Stochastic optimization approaches for elective surgery scheduling with downstream capacity constraints: Models, challenges, and opportunities. *Computers & Operations Research*, 137:105523, 2022.
- [67] Rachee Singh, Sharad Agarwal, Matt Calder, and Paramvir Bahl. Cost-effective cloud edge traffic engineering with cascara. In *18th USENIX Symposium on Networked Systems Design and Implementation (NSDI 21)*, pages 201–216, 2021.
- [68] TeleGeography. Submarine cable map. <https://www.submarinecablemap.com/>, Accessed:2025-04-24.
- [69] Yu Tian, Zhenyu Li, Matthew Yang Liu, Jian Mao, Gareth Tyson, and Gaogang Xie. Cost-saving streaming: Unlocking the potential of alternative edge node resources. In *ACM on Internet Measurement Conference*, pages 580–587, New York, NY, USA, 2024.
- [70] Alexandru Uta, Alexandru Custura, Dmitry Duplyakin, Ivo Jimenez, Jan Rellermeyer, Carlos Maltzahn, Robert Ricci, and Alexandru Iosup. Is big data performance reproducible in modern cloud networks? In *Proceedings of the 17th Usenix Conference on Networked Systems Design and Implementation*, page 513–528, Santa Clara, CA, USA, 2020.
- [71] Greg Van Houdt, Carlos Mosquera, and Gonzalo Nápoles. A review on the long short-term memory model. *Artificial Intelligence Review*, 53(8):5929–5955, 2020.
- [72] Vultr. Cloud compute. <https://www.vultr.com/>, Accessed:2025-04-20.
- [73] Dehui Wei, Jiao Zhang, Haozhe Li, Zhichen Xue, Yajie Peng, Xiaofei Pang, Rui Han, Yan Ma, and Jialin Li. Swarm: Cost-efficient video content distribution with a peer-to-peer system, 2024.
- [74] Sarah Wooders, Shu Liu, Paras Jain, Xiangxi Mo, Joseph E. Gonzalez, Vincent Liu, and Ion Stoica. Cloudcast: High-Throughput, Cost-Aware overlay multicast in the cloud. In *21st USENIX Symposium on Networked Systems Design and Implementation*, pages 281–296, Santa Clara, CA, April 2024.
- [75] Bingyang Wu, Kun Qian, Bo Li, Yunfei Ma, Qi Zhang, Zhigang Jiang, Jiayu Zhao, Dennis Cai, Ennan Zhai, Xuanzhe Liu, and Xin Jin. Xron: A hybrid elastic cloud overlay network for video conferencing at planetary scale. In *Proceedings of the ACM SIGCOMM Conference*, pages 696–709, New York, NY, USA, 2023.
- [76] Zhanghao Wu, Wei-Lin Chiang, Ziming Mao, Zongheng Yang, Eric Friedman, Scott Shenker, and Ion Stoica. Can’t be late: Optimizing spot instance savings under deadlines. In *21st USENIX Symposium on Networked Systems Design and Implementation*, pages 185–203, Santa Clara, CA, April 2024.
- [77] Xbox. Cloud gaming. <https://www.xbox.com/en-US/cloud-gaming>, Accessed:2025-04-24.
- [78] Zhaogui Xu, Ran Ju, Liang Gu, Weiguang Wang, Jin Li, Feng Li, and Lei Han. Using overlay cloud network to accelerate global communications. In *IEEE Conference on Computer Communications Workshops (INFOCOM WKSHPS)*, pages 139–144, 2019.
- [79] Fangkai Yang, Lu Wang, Zhenyu Xu, Jue Zhang, Liquan Li, Bo Qiao, Camille Couturier, Chetan Bansal, Soumya Ram, Si Qin, Zhen Ma, Íñigo Goiri, Eli Cortez, Terry Yang, Victor Rühle, Saravan Rajmohan, Qingwei Lin, and Dongmei Zhang. Snape: Reliable and low-cost computing with mixture of spot and on-demand vms. In *Proceedings of the 28th ACM International Conference on Architectural Support for Programming Languages and Operating Systems, Volume 3*, pages 631–643, New York, NY, USA, 2023.
- [80] Rui-Xiao Zhang, Haiping Wang, Shu Shi, Xiaofei Pang, Yajie Peng, Zhichen Xue, and Jiangchuan Liu. Enhancing resource management of the world’s largest PCDN system for On-Demand video streaming. In *USENIX Annual Technical Conference (USENIX ATC)*, pages 951–965, Santa Clara, CA, July 2024.
- [81] Gongming Zhao, Jingzhou Wang, Hongli Xu, Zhuolong Yu, and Chunming Qiao. Coin: Cost-efficient traffic engineering with various pricing schemes in clouds. In *IEEE INFOCOM 2023-IEEE Conference on Computer Communications*, pages 1–10. IEEE, 2023.

A Lyapunov Drift is Upper Bounded

According to the theory of Lyapunov optimization, we define a quadratic Lyapunov function as a measure of the virtual queue state:

$$L(Q(t)) \triangleq \frac{1}{2} \sum_{k=1}^N w_k Q_k(t)^2, t \in \mathcal{T}. \quad (\text{A-1})$$

A small $L(Q(t))$ leads to small queue backlogs at the time slot t . Then, we introduce the one-slot conditional Lyapunov drift as follows:

$$\Delta(Q(t)) \triangleq \mathbb{E}\{L(Q(t+1)) - L(Q(t)) | Q(t)\}, t \in \mathcal{T}. \quad (\text{A-2})$$

We obtain the inequality:

$$\Delta(Q(t)) < B + \sum_{k=1}^N w_k Q_k(t) \delta \text{cpu}_k^{t,\text{in}} \quad (\text{A-3})$$

where $B = \frac{1}{2} \sum_{k=1}^N w_k y_{\max}^2$, and y_{\max} is the upper limit of the queue increment magnitude. Next, we start to prove (A-3).

From equation (A-1), we have:

$$Q_k(t+1) = \max[Q_k(t) + \text{cpu}_k^{t,\text{onset}} + \delta \text{cpu}_k^{t,\text{in}} - \theta, 0] \quad (\text{A-4})$$

Squaring both sides and noting that $\max[x, 0]^2 \leq x^2$:

$$Q_k(t+1)^2 \leq (Q_k(t) + \text{cpu}_k^{t,\text{onset}} + \delta \text{cpu}_k^{t,\text{in}} - \theta)^2 \quad (\text{A-5})$$

Expanding the right side:

$$Q_k(t+1)^2 \leq Q_k(t)^2 + (\text{cpu}_k^{t,\text{onset}} + \delta \text{cpu}_k^{t,\text{in}} - \theta)^2 + 2Q_k(t)(\text{cpu}_k^{t,\text{onset}} + \delta \text{cpu}_k^{t,\text{in}} - \theta) \quad (\text{A-6})$$

Using the telescoping sum in (A-6), along with the definitions of the Lyapunov function (A-1) and Lyapunov drift (A-2), we obtain:

$$\begin{aligned} \Delta(Q(t)) &\leq \frac{1}{2} \sum_{k=1}^N w_k \mathbb{E}\{(\text{cpu}_k^{t,\text{onset}} + \delta \text{cpu}_k^{t,\text{in}} - \theta)^2 | Q(t)\} \\ &\quad + \sum_{k=1}^N w_k Q_k(t) \mathbb{E}\{(\text{cpu}_k^{t,\text{onset}} + \delta \text{cpu}_k^{t,\text{in}} - \theta) | Q(t)\} \end{aligned} \quad (\text{A-7})$$

Due to system physical constraints $\text{cpu}_k^{t,\text{onset}} \in [0, 100\%]$, $\delta \text{cpu}_k^{t,\text{in}}$ is bounded and θ is constant, there exists y_{\max} such that:

$$(\text{cpu}_k^{t,\text{onset}} + \delta \text{cpu}_k^{t,\text{in}} - \theta)^2 \leq y_{\max}^2 \quad (\text{A-8})$$

By defining $B = \frac{1}{2} \sum_{k=1}^N w_k y_{\max}^2$, we obtain:

$$\Delta(Q(t)) < B + \sum_{k=1}^N w_k Q_k(t) \mathbb{E}\{(\text{cpu}_k^{t,\text{onset}} + \delta \text{cpu}_k^{t,\text{in}} - \theta) | Q(t)\} \quad (\text{A-9})$$

Noting what $\mathbb{E}\{(\text{cpu}_k^{t,\text{onset}} - \theta) | Q(t)\}$ is known given $Q(t)$, and focusing on the control variable $\delta \text{cpu}_k^{t,\text{in}}$, we derive the final form:

$$\Delta(Q(t)) < B + \sum_{k=1}^N w_k Q_k(t) \delta \text{cpu}_k^{t,\text{in}} \quad (\text{A-10})$$

This establishes that all queues are mean rate stable, i.e.,

$\lim_{t \rightarrow \infty} \frac{\mathbb{E}\{Q(t)\}}{t} = 0$, with the proof relying on the results from [Appendix B](#). The complete proof is provided in [Appendix C](#).

B Computable Form of the DPP

To prove that **P1** can transform into **P2**, we establish the following lemma:

Lemma 1: For the drift-plus-penalty approach, the problem

$$\mathbf{P1} : \min(\Delta(Q(t)) + V \cdot \mathbb{E}\{\text{delay}(t) | Q(t)\}) \quad (\text{B-1})$$

can be transformed by minimizing its upper bound.

Proof: From Appendix A, we have:

$$\Delta(Q(t)) < B + \sum_{k=1}^N w_k Q_k(t) \delta \text{cpu}_k^{t,\text{in}} \quad (\text{B-2})$$

Adding the penalty term:

$$\begin{aligned} \Delta(Q(t)) + V \cdot \mathbb{E}\{\text{delay}(t) | Q(t)\} &< B + \\ &\sum_{k=1}^N w_k Q_k(t) \delta \text{cpu}_k^{t,\text{in}} + V \cdot \mathbb{E}\{\text{delay}(t) | Q(t)\} \end{aligned} \quad (\text{B-3})$$

The penalty term can be expressed as:

$$\mathbb{E}\{\text{delay}(t) | Q(t)\} = \mathbb{E}\left\{\sum_{k=1}^N \text{delay}_k' \cdot \delta \text{req}_k^{t,\text{in}} | Q(t)\right\} \quad (\text{B-4})$$

Substituting (B-4) into (B-3):

$$\begin{aligned} \Delta(Q(t)) + V \cdot \mathbb{E}\{\text{delay}(t) | Q(t)\} &< B + \\ &\sum_{k=1}^N w_k Q_k(t) \delta \text{cpu}_k^{t,\text{in}} + V \cdot \sum_{k=1}^N \text{delay}_k' \cdot \delta \text{req}_k^{t,\text{in}} \end{aligned} \quad (\text{B-5})$$

Since B is a constant, minimizing the right side of (B-5) leads to:

$$\mathbf{P2} : \min_{\delta \text{req}_k^{t,\text{in}}} \sum_{k=1}^N \left(w_k Q_k(t) \cdot \delta \text{cpu}_k^{t,\text{in}} + V \cdot \text{delay}_k' \cdot \delta \text{req}_k^{t,\text{in}} \right) \quad (\text{B-6})$$

This establishes the transformation from **P1** to **P2**, completing the proof. ■

C All Queues Q_k Are Mean Rate Stable

In this section, we will prove that all queues are mean rate stable.

Lemma 2: The solution to **P2** ensures queue stability.

Proof:

We first make two critical assumptions:

Assumption 1: There exists an alternative feasible strategy $\delta \text{req}_k^{t,\text{in,alt}}$ that satisfies:

$$\mathbb{E}\{(\text{cpu}_k^{t,\text{onset}} + \delta \text{cpu}_k^{t,\text{in,alt}} - \theta) | Q(t)\} \leq -\varepsilon, \forall k \in \{1, \dots, N\} \quad (\text{C-1})$$

where $\varepsilon > 0$.

Assumption 2: The delay function is bounded:

$$\exists \text{delay}_{\min}, \text{delay}_{\max} \in \mathbb{R}, \forall k, t : \text{delay}_{\min} \leq \text{delay}_k^t \leq \text{delay}_{\max} \quad (\text{C-2})$$

We derive the drift bound using our optimal control solution $\delta \text{cpu}_k^{t, \text{in}, *}$:

$$\begin{aligned} \Delta(Q(t)) &\leq B + \sum_{k=1}^N w_k Q_k(t) \mathbb{E}\{(\text{cpu}_k^{t, \text{onset}} + \delta \text{cpu}_k^{t, \text{in}, *} - \theta) | Q(t)\} \\ &\leq B + \sum_{k=1}^N w_k Q_k(t) \mathbb{E}\{\delta \text{cpu}_k^{t, \text{in}, *} | Q(t)\} \\ &\quad + \sum_{k=1}^N w_k Q_k(t) (\text{cpu}_k^{t, \text{onset}} - \theta) \end{aligned} \quad (\text{C-3})$$

By the optimality of our solution to **P2** and using our alternative strategy:

$$\begin{aligned} \sum_{k=1}^N w_k Q_k(t) \cdot \delta \text{cpu}_k^{t, \text{in}, *} &\leq \sum_{k=1}^N w_k Q_k(t) \cdot \delta \text{cpu}_k^{t, \text{in}, \text{alt}} \\ &\quad + V \sum_{k=1}^N \text{delay}_k^t (\delta \text{req}_k^{t, \text{in}, \text{alt}} - \delta \text{req}_k^{t, \text{in}, *}) \end{aligned} \quad (\text{C-4})$$

Substituting (C-4) into (A-9):

$$\begin{aligned} \Delta(Q(t)) &\leq B + \sum_{k=1}^N w_k Q_k(t) (\text{cpu}_k^{t, \text{onset}} - \theta) \\ &\quad + \sum_{k=1}^N w_k Q_k(t) \mathbb{E}\{\delta \text{cpu}_k^{t, \text{in}, \text{alt}} | Q(t)\} \\ &\quad + V \sum_{k=1}^N \text{delay}_k^t (\delta \text{req}_k^{t, \text{in}, \text{alt}} - \delta \text{req}_k^{t, \text{in}, *}) \end{aligned} \quad (\text{C-5})$$

Using **Assumption 1** and bounded delay (**Assumption 2**) properties:

$$\begin{aligned} \Delta(Q(t)) &\leq B + \sum_{k=1}^N w_k Q_k(t) (\text{cpu}_k^{t, \text{onset}} - \theta) \\ &\quad - \epsilon \sum_{k=1}^N w_k |Q_k(t)| + V \cdot C \\ &\leq B + V \cdot C - \epsilon \sum_{k=1}^N w_k |Q_k(t)| \end{aligned} \quad (\text{C-6})$$

where $C = \text{delay}_{\max} - \text{delay}_{\min}$ is bounded.

Let $B' = B + V \cdot C$. Then:

$$\Delta(Q(t)) \leq B' - \epsilon \sum_{k=1}^N w_k |Q_k(t)| \quad (\text{C-7})$$

Taking the expectations of both sides:

$$\mathbb{E}\{\Delta(Q(t))\} \leq B' - \epsilon \sum_{k=1}^N w_k \mathbb{E}\{|Q_k(t)|\} \quad (\text{C-8})$$

Summing over time slots $t \in \{0, \dots, T-1\}$:

$$\sum_{t=0}^{T-1} \mathbb{E}\{\Delta(Q(t))\} \leq B'T - \epsilon \sum_{t=0}^{T-1} \sum_{k=1}^N w_k \mathbb{E}\{|Q_k(t)|\} \quad (\text{C-9})$$

By definition of Lyapunov drift (A-2) and telescoping sums:

$$\mathbb{E}\{L(Q(T))\} - \mathbb{E}\{L(Q(0))\} \leq B'T - \epsilon \sum_{t=0}^{T-1} \sum_{k=1}^N w_k \mathbb{E}\{|Q_k(t)|\} \quad (\text{C-10})$$

Since $\mathbb{E}\{L(Q(T))\} \geq 0$ and $\mathbb{E}\{L(Q(0))\} = 0$:

$$\epsilon \sum_{t=0}^{T-1} \sum_{k=1}^N w_k \mathbb{E}\{|Q_k(t)|\} \leq B'T \quad (\text{C-11})$$

Then, we can derive:

$$\mathbb{E}\{L(Q(T))\} \leq B'T \quad (\text{C-12})$$

Substituting (C-12) into the Lyapunov function (A-1) gives:

$$\frac{1}{2} \sum_{k=1}^N w_k \mathbb{E}\{Q_k(T)^2\} \leq B'T \quad (\text{C-13})$$

By the *Cauchy-Schwarz inequality*, here we denote $\min_k w_k$ the minimum weight among all queues, which gives us the most conservative bound:

$$\left(\sum_{k=1}^N \mathbb{E}\{Q_k(T)\} \right)^2 \leq N \sum_{k=1}^N \mathbb{E}\{Q_k(T)^2\} \leq \frac{2NB'T}{\min_k w_k} \quad (\text{C-14})$$

Taking the square root and dividing by T :

$$\frac{\sum_{k=1}^N \mathbb{E}\{Q_k(T)\}}{T} \leq \sqrt{\frac{2NB'}{T \min_k w_k}} \quad (\text{C-15})$$

Taking the limit as $T \rightarrow \infty$:

$$\lim_{T \rightarrow \infty} \frac{\sum_{k=1}^N \mathbb{E}\{Q_k(T)\}}{T} = 0 \quad (\text{C-16})$$

Since $Q_k(T) \geq 0$ for all k , we have:

$$\lim_{T \rightarrow \infty} \frac{\mathbb{E}\{Q_k(T)\}}{T} = 0, \forall k \in \{1, \dots, N\} \quad (\text{C-17})$$

Therefore, all queues are mean rate stable, ensuring that our algorithm satisfies the constraints of the original problem. \blacksquare

D Supplementary Evaluation Results

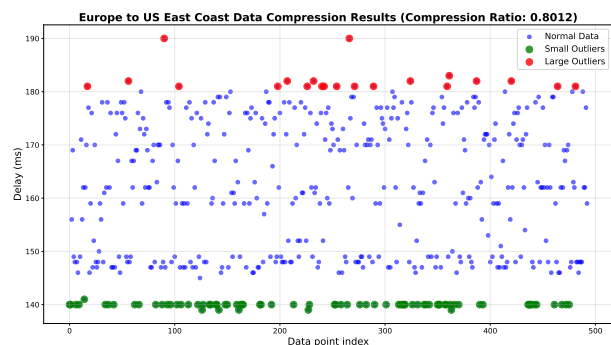


Fig. 17. Data Compression in Europe and the US East.

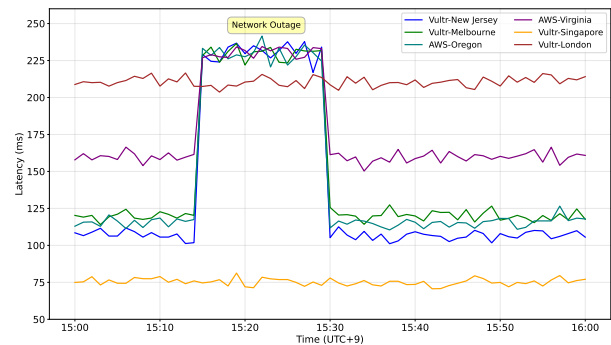


Fig. 18. Probing Data Display for the GCP-Tokyo Node.

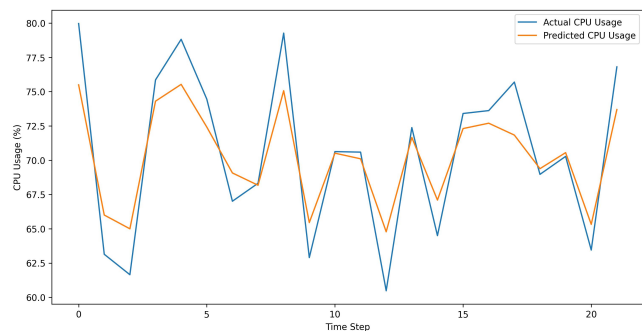


Fig. 19. LSTM-Driven CPU Forecasting.